A&A 446, 361–366 (2006)
DOI: 10.1051/0004-6361:20053631

Astronomy & Astrophysics

Atomic data from the IRON project

LX. Electron-impact excitation of $n = 3, 4$ levels of Fe^{17+}

M. C. Witthoeft[1], N. R. Badnell[1], G. Del Zanna[2], K. A. Berrington[3], and J. C. Pelan[4]

[1] Department of Physics, University of Strathclyde, Glasgow, G4 0NG, UK
e-mail: witthoeft@phys.strath.ac.uk
[2] MSSL, University College London, Holmbury St., Mary Dorking, RH5 6NT, UK
[3] School of Science and Mathematics, Sheffield Hallam University, Sheffield, S1 1WB, UK
[4] Gatsby Computational Neuroscience Unit, University College, 17 Queen Square, London, WC1N 3AR, UK

Received 14 June 2005 / Accepted 1 September 2005

ABSTRACT

We present results for electron-impact excitation of F-like Fe calculated using *R*-matrix theory where an intermediate-coupling frame transformation (ICFT) is used to obtain level-resolved collision strengths. Two such calculations are performed, the first expands the target using $2s^2\ 2p^5$, $2s\ 2p^6$, $2s^2\ 2p^4 3l$, $2s\ 2p^5 3l$, and $2p^6 3l$ configurations while the second calculation includes the $2s^2\ 2p^4 4l$, $2s\ 2p^5 4l$, and $2p^6 4l$ configurations as well. The effect of the additional structure in the latter calculation on the $n = 3$ resonances is explored and compared with previous calculations. We find strong resonant enhancement of the effective collision strengths to the $2s^2\ 2p^4\ 3s$ levels. A comparison with a Chandra X-ray observation of Capella shows that the $n = 4$ *R*-matrix calculation leads to good agreement with observation.

Key words. atomic data – atomic processes

1. Introduction

This work is a continuation of research done as part of the IRON Project (Hummer et al. 1993) whose goal is to provide accurate atomic data for astrophysically relevant elements, particularly iron, using the most sophisticated computational methods to date. The focus of this work is the calculation of all fine-structure collision strengths of electron-impact excitation of Fe^{17+} for single-promotion transitions from the ground level up to the $n = 4$ levels and all transitions between them. An investigation is made examining the difference between this calculation and a smaller calculation, also performed as part of this work, which only considers excited states with $n \leq 3$. These studies consist of direct comparisons of collision strengths and effective collision strengths as well as simulated emission spectra of a low density astrophysical plasma.

Previous works on this ion consist of distorted wave calculations by Mann (1983) and Cornille et al. (1992), a relativistic distorted wave calculation of Sampson et al. (1991), and a non-relativistic *R*-matrix calculation of Mohan et al. (1987) which included the $2s^2\ 2p^5$, $2s\ 2p^6$, and $2s^2\ 2p^4 3l$ terms. A previous IRON Project report, IP XXVIII (Berrington et al. 1998), examined, using *R*-matrix theory, just the fine structure transition of the ground term, $^2P_{3/2} \rightarrow {}^2P_{1/2}$, for several F-like ions including Fe using the same target expansion as the present $(n = 3)$-state calculation.

The rest of this paper is organized as follows. In Sect. 2, the details of the present calculations will be discussed including a comparison of our target structure with other calculations and experimental measurements. In Sect. 3, we examine the collision strengths and simulated emission spectra of the present calculations and perform comparisons with other calculations and observations. Finally, in Sect. 4, we provide a brief summary of the results.

2. Calculation

As mentioned before, two *R*-matrix calculations are performed for this report. The intermediate-coupling frame transformation (ICFT) method of Griffin et al. (1998) using multi-channel quantum defect theory (MQDT) is utilized to enable us to perform much of the calculation in *LS* coupling. The advantage of this approach is realized in the diagonalization time of the $(N + 1)$-electron Hamiltonian whose size is determined by the number of *LS* terms and not the larger number of *jK* levels. In the smaller $(n = 3)$-state calculation we include the $2s^2\ 2p^5$, $2s\ 2p^6$, $2s^2\ 2p^4 3l$, $2s\ 2p^5 3l$, and $2p^6 3l$ configurations which have a total of 52 terms containing 113 fine-structure levels. The second calculation is an extension of the first adding the $2s^2\ 2p^4 4l$, $2s\ 2p^5 4l$, and $2p^6 4l$ configurations to the target expansion. This results in a total of 124 terms and 279 levels.

Table 1. Radial scaling factors used in AUTOSTRUCTURE to minimize the total energy of the *nl* orbital wave functions.

	$n = 3$	$n = 4$
λ_{1s}	1.3895	1.3923
λ_{2s}	1.1971	1.2076
λ_{2p}	1.1313	1.1404
λ_{3s}	1.1315	1.1266
λ_{3p}	1.0857	1.0807
λ_{3d}	1.1223	1.1122
λ_{4s}	–	1.1219
λ_{4p}	–	1.0807
λ_{4d}	–	1.1077
λ_{4f}	–	1.1133

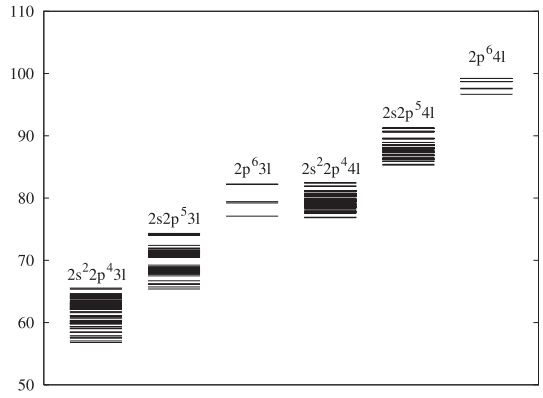

Fig. 1. Energy levels in Ry for the $n = 4$ structure calculation from AUTOSTRUCTURE.

The target structure and resulting wave functions are calculated using AUTOSTRUCTURE (see Badnell 1986) where a radial scaling parameter, λ_{nl}, of each orbital is varied to minimize the average energy of each term. The radial scaling parameters used for both calculations are given in Table 1. The $n = 3$ level energies do not change significantly by the addition of the $n = 4$ levels in the larger calculation. The reason for this is demonstrated in Fig. 1 where the energy levels for the $n = 4$ calculation are displayed. The only overlap between the $n = 3$ and $n = 4$ levels is between the $2p^6 3l$ and $2s^2\ 2p^4 4l$ levels. Since only three-electron transitions connect these levels, this overlap does not have a significant effect on the level energies. In Table 2 we list the energies of the lowest 66 levels from the $n = 4$ calculation, compared to those of the version 3 of the NIST database (see `http://physics.nist.gov`). Since the level energies of the $n = 3$ calculation are within 0.1% of the $n = 4$ calculation they are not shown. With the exception of the first two excited states, which disagree by 2% and 1% respectively, all our level energies agree with the measurements listed on NIST to within 0.6% except for levels 33 and 34. We shall subsequently refer to levels using the energy ordered index given in this table.

As a further test of the target structure, we compare our oscillator strengths with previous calculations. In Table 3 we list the oscillator strengths from both our $n = 3$ and $n = 4$ calculations with the SUPERSTRUCTURE calculation of Cornille et al. (1992), the relativistic atomic structure calculation by Sampson et al. (1991), and finally the relativistic Hartree-Fock calculation of Fawcett (1984), which included semi-empirical corrections. There is generally good agreement between all the calculations.

Both the $n = 3$ and $n = 4$ R-matrix calculations include the mass-velocity and Darwin relativistic corrections and include a total of 20 continuum terms per channel. We performed a full-exchange calculation for $J \leq 10$ and a non-exchange calculation to provide the contributions up to $J = 38$. A further top-up was done using the Burgess sum rule (see Burgess 1974) for dipole transitions and using a geometric series for the non-dipole transitions with care taken to ensure smooth convergence towards the high energy limiting points (see Badnell & Griffin 2001; Whiteford et al. 2001 for a detailed discussion). In the outer region, we calculated the collision strengths up to an electron-impact energy of 200 Ry with the following energy spacings: $10^{-5}z^2$ Ry in regions with strong resonance contributions; $10^{-4}z^2$ Ry for the region between the $n = 2$ and $n = 3$ resonances; and $10^{-3}z^2$ Ry for high energies outside the resonance region. Although this energy mesh does not resolve all resonances, we consider the more than 15 000 energy points to be sufficient to accurately sample the small width resonances, as discussed by Badnell & Griffin (2001). Effective collision strengths at high temperatures are obtained for dipole and Born allowed transitions by interpolation between the R-matrix calculation at 200 Ry and an infinite energy point calculated by AUTOSTRUCTURE, following the methods described in Burgess et al. (1997) and Chidichimo et al. (2003).

3. Results

3.1. Ordinary and effective collision strengths

Overall, the differences between the results of the $n = 3$ and $n = 4$ calculations are small, particularly for the strong transitions. In Fig. 2, we compare the collision strength of both calculations for the ground state fine structure transition (1–2) and find that there are only small differences in the resonant structure. Figure 3 shows the net effect of those small differences on the effective collision strength. Also shown are the results of a previous R-matrix calculation (Berrington et al. 1998) which is performed in LS-coupling and includes the same target expansion as our $n = 3$ ICFT calculation. Differences between the effective collision strengths of two present calculations are around 10% for all temperatures shown and are in good agreement with the results of Berrington et al.

Next we examine the transition to the first $2p^4\ 3s$ level (1–4) in Figs. 4 and 5. In Fig. 4, again there are only small differences in the resonance structure of the $n = 3$ transitions. We also observe that the additional $n = 4$ resonances appearing beyond 10 Ry in the larger calculation are small and do not contribute much to the effective collision strength, which we show in Fig. 5 along with the results of the R-matrix calculation of Mohan et al. (1986) and the relativistic distorted wave calculation of Sampson et al. (1991). Again we see that differences between the present results are on the order of 10%. The two previous calculations give appreciably smaller effective collision strengths for this transition especially at low temperatures.

Table 2. Lowest 66 energy levels in Ry for the $n = 4$ calculation compared to experimental measurements listed on NIST (`http://physics.nist.gov`).

i	Level	Present	NIST	i	Level	Present	NIST	i	Level	Present	NIST
1	$2p^5\ ^2P^o_{3/2}$	0.0	0.0	23	$2p^4\ 3p\ ^2S^o_{1/2}$	60.309		45	$2p^4\ 3d\ ^4F_{7/2}$	63.111	
2	$2p^5\ ^2P^o_{1/2}$	0.955	0.935	24	$2p^4\ 3p\ ^2D^o_{3/2}$	60.356		46	$2p^4\ 3d\ ^2D_{3/2}$	63.140	
3	$2s\ 2p^6\ ^2S_{1/2}$	9.830	9.702	25	$2p^4\ 3p\ ^2F^o_{5/2}$	60.693		47	$2p^4\ 3d\ ^4P_{5/2}$	63.297	62.911
4	$2p^4\ 3s\ ^4P_{5/2}$	56.798	56.699	26	$2p^4\ 3p\ ^2F^o_{7/2}$	60.878		48	$2p^4\ 3d\ ^2P_{3/2}$	63.418	63.308
5	$2p^4\ 3s\ ^2P_{3/2}$	57.052	56.937	27	$2p^4\ 3p\ ^2D^o_{3/2}$	61.016		49	$2p^4\ 3d\ ^2D_{5/2}$	63.516	63.401
6	$2p^4\ 3s\ ^4P_{1/2}$	57.492	57.503	28	$2p^4\ 3p\ ^2D^o_{5/2}$	61.126		50	$2p^4\ 3d\ ^2G_{7/2}$	63.787	
7	$2p^4\ 3s\ ^4P_{3/2}$	57.664	57.573	29	$2p^4\ 3p\ ^2P^o_{3/2}$	61.590		51	$2p^4\ 3d\ ^2G_{9/2}$	63.825	
8	$2p^4\ 3s\ ^2P_{1/2}$	57.899	57.798	30	$2p^4\ 3p\ ^2P^o_{1/2}$	61.758		52	$2p^4\ 3d\ ^2F_{5/2}$	64.052	
9	$2p^4\ 3s\ ^2D_{5/2}$	58.444	58.321	31	$2p^4\ 3d\ ^4D_{5/2}$	62.114		53	$2p^4\ 3d\ ^2S_{1/2}$	64.056	63.919
10	$2p^4\ 3s\ ^2D_{3/2}$	58.478	58.356	32	$2p^4\ 3d\ ^4D_{7/2}$	62.127		54	$2p^4\ 3d\ ^2F_{7/2}$	64.156	
11	$2p^4\ 3p\ ^4P^o_{3/2}$	59.019		33	$2p^4\ 3d\ ^4D_{3/2}$	62.157	63.051	55	$2p^4\ 3d\ ^2P_{3/2}$	64.280	64.139
12	$2p^4\ 3p\ ^4P^o_{5/2}$	59.053		34	$2p^4\ 3d\ ^4D_{1/2}$	62.247	62.907	56	$2p^4\ 3d\ ^2D_{5/2}$	64.335	64.160
13	$2p^4\ 3p\ ^4P^o_{1/2}$	59.296		35	$2p^4\ 3p\ ^2P^o_{3/2}$	62.335		57	$2p^4\ 3d\ ^2D_{3/2}$	64.558	64.391
14	$2p^4\ 3p\ ^4D^o_{7/2}$	59.350		36	$2p^4\ 3d\ ^4F_{9/2}$	62.356		58	$2p^4\ 3d\ ^2P_{1/2}$	64.623	64.465
15	$2p^4\ 3p\ ^2D^o_{5/2}$	59.365		37	$2p^4\ 3d\ ^2F_{7/2}$	62.452		59	$2p^4\ 3d\ ^2D_{5/2}$	65.356	65.305
16	$2p^4\ 3s\ ^2S_{1/2}$	59.807	59.917	38	$2p^4\ 3p\ ^2P^o_{1/2}$	62.542		60	$2s2p^5\ 3s\ ^4P^o_{5/2}$	65.396	65.482
17	$2p^4\ 3p\ ^4D^o_{1/2}$	59.810		39	$2p^4\ 3d\ ^4P_{1/2}$	62.597	62.497	61	$2p^4\ 3d\ ^2D_{3/2}$	65.542	65.468
18	$2p^4\ 3p\ ^4D^o_{3/2}$	59.840		40	$2p^4\ 3d\ ^4P_{3/2}$	62.734	62.626	62	$2s\ 2p^5\ 3s\ ^4P^o_{3/2}$	65.726	65.591
19	$2p^4\ 3p\ ^2P^o_{1/2}$	59.844		41	$2p^4\ 3d\ ^2F_{5/2}$	62.816	62.699	63	$2s\ 2p^5\ 3s\ ^4P^o_{1/2}$	66.140	65.835
20	$2p^4\ 3p\ ^2P^o_{3/2}$	59.980		42	$2p^4\ 3d\ ^2P_{1/2}$	62.957		64	$2s\ 2p^5\ 3s\ ^2P^o_{3/2}$	66.221	66.075
21	$2p^4\ 3p\ ^4D^o_{5/2}$	60.124		43	$2p^4\ 3d\ ^4F_{3/2}$	62.989		65	$2s\ 2p^5\ 3s\ ^2P^o_{1/2}$	66.709	
22	$2p^4\ 3p\ ^4S^o_{3/2}$	60.157		44	$2p^4\ 3d\ ^4F_{5/2}$	63.012		66	$2s\ 2p^5\ 3p\ ^4S_{3/2}$	67.505	

Table 3. Comparison of various calculated gf-values for the present calculations with Cornille et al. (1992), Sampson et al. (1991), and Fawcett (1984).

trans	$n = 3$	$n = 4$	Cornille	Sampson	Fawcett
1–4	0.0197	0.0198	0.020	0.0172	0.021
1–5	0.2409	0.2419	0.247	0.2184	0.280
2–5	0.0063	0.0062	0.006	0.0056	0.007
1–6	0.0136	0.0136	0.010	0.0136	0.015
2–6	0.0004	0.0004	–	0.0004	–
1–10	0.0023	0.0024	0.003	0.0024	0.005
2–10	0.1789	0.1818	0.185	0.1646	0.200
1–43	0.0892	0.0887	0.057	0.0912	0.097
2–43	0.0093	0.0094	0.009	0.0108	0.008
1–58	0.2826	0.2683	0.284	0.2968	0.272
2–58	1.383	1.356	1.40	1.294	1.386

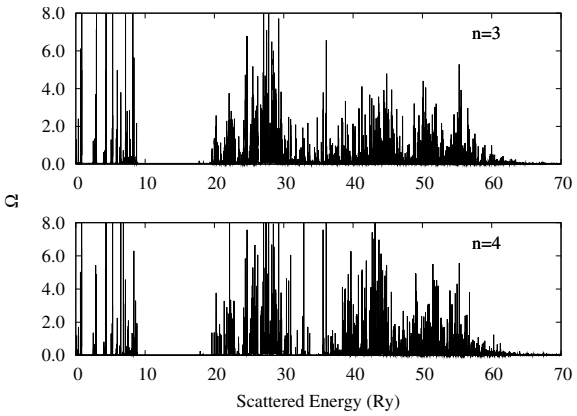

Fig. 2. Collision strengths versus scattered electron energy for the $n = 3$ (*top*) and $n = 4$ (*bottom*) ICFT calculations of the 1–2 transition.

The same occurs for the other transitions to the $2p^4\ 3s$ levels. In the case of the Mohan et al. results, this difference demonstrates the importance of the $2s\ 2p^5 3l$ terms on transitions involving the $2s^2\ 2p^4 3l$ levels.

In Fig. 6, we directly compare the effective collision strengths of the $n = 3$ and $n = 4$ calculations for transitions from either level of the ground state term at a temperature of $\log T = 6.81$. The strength of each transition plotted is given by its position in the figure; the horizontal position gives the effective collision strength from the $n = 3$ calculation while the vertical position gives the effective collision strength as determined by the $n = 4$ calculation. The solid line marks where the results of both calculations agree. We find that, for the strong transitions, the agreement between the results of the two calculations is good while the $n = 4$ calculation gives consistently larger effective collision strengths for the weaker transitions. For the weakest transitions, the effective collision strengths can differ by a factor of 5. It must also be noted that, as the temperature is increased, the agreement between the two sets of results improves rapidly for the weaker transitions.

Since plane-wave Born calculations are often used as baseline data, especially for complex systems, it is also instructive to perform a similar comparison between the present $n = 4$ R-matrix calculation and an $n = 4$ plane-wave Born calculation (Burgess et al. 1997). The Born calculation has been modified

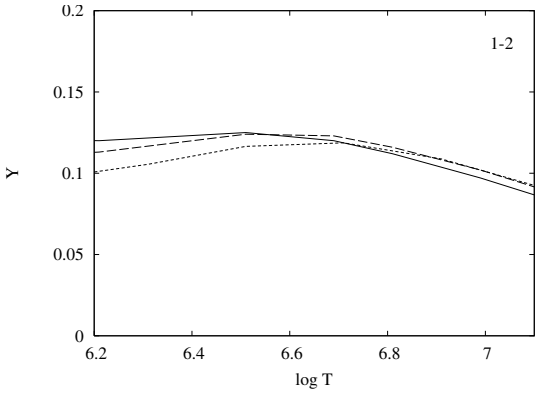

Fig. 3. Effective collision strengths of the 1–2 transition comparing the present $n = 3$ calculation (solid), $n = 4$ calculation (dashed) and an $n = 3$ R-matrix calculation by Berrington et al. (1998) (dotted).

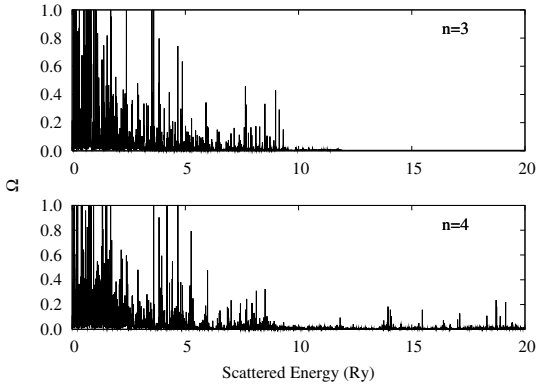

Fig. 4. Collision strengths versus scattered electron energy for the $n = 3$ (*top*) and $n = 4$ (*bottom*) ICFT calculations of the 1–4 transition.

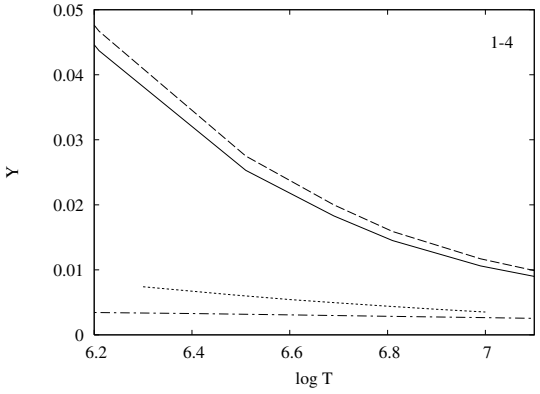

Fig. 5. Effective collision strengths of the 1–4 transition comparing the present $n = 3$ calculation (solid), $n = 4$ calculation (dashed), the $n = 3$ R-matrix calculation by Mohan et al. (1987) (dotted) and the distorted wave calculation of Sampson et al. (1991) (dot-dashed).

to ensure a non-zero collision strength at threshold (see Cowan 1981, p. 569). Transitions from both $2s^2\ 2p^5$ levels at a temperature of $\log T = 6.81$ are shown in Fig. 7. We find that, while the Born calculation gives quite good results for the strongest transitions, it can severely underestimate the strength of the weaker transitions by several orders of magnitude. The reason for this is illustrated in Fig. 8 where both the collision strengths and effective collision strengths are shown for the two

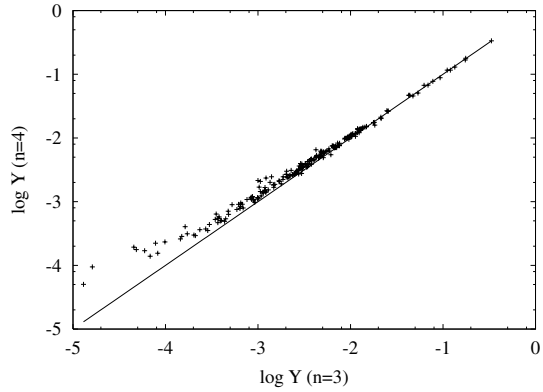

Fig. 6. Comparison of effective collisions strengths for transitions from the $2s^2\ 2p^5$ levels for the present $n = 3$ and $n = 4$ ICFT calculations at a temperature of $\log T = 6.81$.

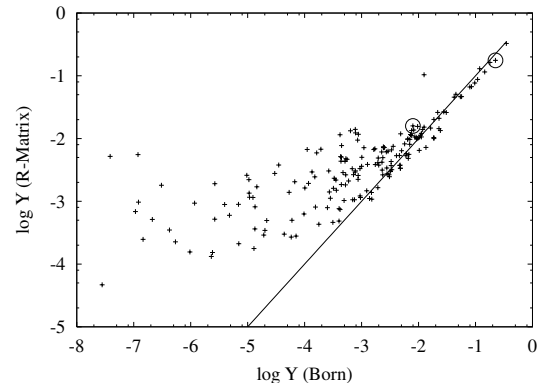

Fig. 7. Comparison of effective collision strengths for transitions from the $2s^2\ 2p^5$ levels for the present $n = 4$ ICFT calculation and an $n = 4$ Born calculation at a temperature of $\log T = 6.81$. The circled transitions are marked for discussion in the text.

transitions circled in Fig. 7. The effective collision strength of the stronger 1–56 transition, shown in the top row of Fig. 8, is seen to be dominated by the background and the resonant enhancement has little net effect. In fact, the effective collision strength is nearly indistinguishable from the background for this very strong transition. In the bottom row of Fig. 8, we see that the background of the 1–9 transition is small and the effective collision strength is significantly affected by the strong resonant enhancement. Transitions weaker than the 1–9 transition are even more dominated by resonant enhancement which explains the large discrepancy between the Born and R-Matrix results seen in Fig. 7. At larger temperatures, resonant enhancement contributes less to the effective collision strength and there is better agreement between the Born and R-Matrix results.

3.2. Simulated emission spectra

It is useful to use the data from the present calculations to model a low density Fe^{17+} plasma to obtain radiative emission spectra which can be compared directly with observations. To best examine differences in the calculations, we have chosen to model a steady-state plasma dominated by collisional excitations which is suitable for a wide range of astrophysical

Table 4. List of the most prominent $n = 3$ to $n = 2$ transitions. The columns indicate: (1) the observed wavelength; (2) transition; (3) the line ratio of observation using the high-energy grating on Chandra (Desai et al. 2005); (4, 5) the $n = 4$ R-matrix results for $\log T = 6.6$ and 6.8 respectively; (6) ratio of poulation of upper level due to radiative cascade to the population due to direct excitation for the $n = 4$ R-matrix calculation; (7–9) the same as Cols. (4–6) but for the $n = 3$ R-matrix calculation; (10, 11) APEC (version 1.10) intensities for $\log T = 6.6, 6.8$; (12) Desai et al. (2005) using an emission measure distribution peaked at $\log T = 6.8$; (13) intensity ratios calculated using the distorted wave collision strengths of Sampson et al. (1991). Note: the 16.076 Å feature was measured by both a high-energy grating (HEG) and a medium-energy grating (MEG) which gave different results; the value in parentheses is from the MEG.

λ (Å)	Trans.	Iobs	$I(n = 4)$	$C(n = 4)$	$I(n = 3)$	$C(n = 3)$	I(APEC (Desai))	I(DW $n = 3$)
14.208	56–1 (3d–2p)		0.64–0.64	0.01	0.65–0.65	<0.01	0.65–0.65 (0.65)	0.65–0.65
14.208	55–1 (3d–2p)	1.0	0.36–0.36	0.01	0.35–0.35	<0.01	0.35–0.35 (0.35)	0.35–0.35
14.261	53–1 (3d–2p)		0.15–0.15	0.02	0.14–0.14	<0.01	0.13–0.13 (0.13)	0.12–0.12
14.261	52–1 (3d–2p)	0.30	0.06–0.06	0.12	0.05–0.05	0.07	0.06–0.06 (0.08)	0.06–0.05
14.376	49–1 (3d–2p)	0.39	0.27–0.26	0.04	0.25–0.24	0.02	0.26–0.25 (0.26)	0.24–0.23
14.539	41–1 (3d–2p)	0.28	0.21–0.20	0.12	0.18–0.17	0.07	0.19–0.19 (0.19)	0.18–0.18
15.628	9–1 (3s–2p)	0.31	0.44–0.34	3.2	0.32–0.24	2.5	0.26–0.25 (0.27)	0.17–0.16
15.870	7–1 (3s–2p)	0.21	0.31–0.23	2.9	0.22–0.16	2.4	0.16–0.15 (0.17)	0.11–0.10
15.870	10–2 (3s–2p)	0.24 (bl)	0.18–0.13	2.9	0.12–0.08	2.2	0.08–0.08 (0.09)	0.05–0.04
16.008	5–1 (3s–2p)	0.58 (bl)	0.50–0.38	3.6	0.36–0.27	2.8	0.30–0.28 (0.71?)	0.20–0.17
16.076	4–1 (3s–2p)	0.71(0.59)	0.83–0.60	6.5	0.60–0.42	5.0	0.40–0.34 (0.39)	0.32–0.25

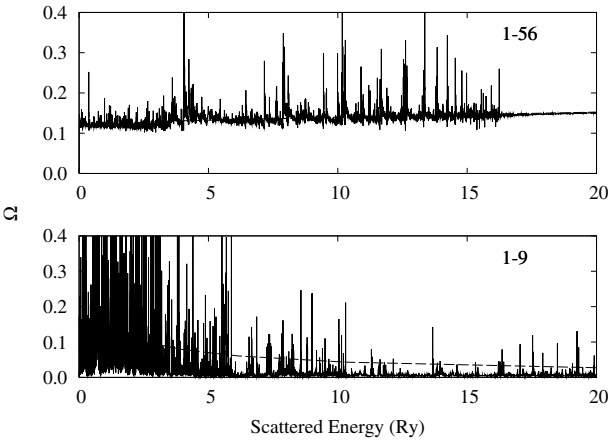

Fig. 8. Collision strengths and effective collision strengths for the 1–56 (*top*) and 1–9 (*bottom*) transitions. The effective collision strength is given as the dashed curve.

applications. The level populations have been calculated taking into account all collisional and radiative processess between the levels. Recently, Desai et al. (2005) pointed out discrepancies between the Capella line intensities obtained by Chandra and those calculated with an emission measure distribution, and the ion model included in the Astrophysical Plasma Emission Code (APEC). Table 4 presents a comparison between these observations (the observed line intensities have been normalised to the brightest line) and various ion models. The intensity ratios calculated with the $n = 3, 4$ R-matrix data are presented in the table, together with those that we have obtained from the APEC database version 1.10. We note that the APEC ion model contains distorted wave collisional data up to $n = 5$ obtained with HULLAC. In addition to the present ICFT $n = 3$ and $n = 4$ calculations we have built, as a representative distorted wave calculation, another $n = 3$ ion model which uses the same radiative data, and the collision strengths of Sampson et al. (1991) (obtained from the CHIANTI[1] database version 4). This is referred in Table 4 as DW $n = 3$. We note that the radiative data (wavelengths and A-values) between the R-matrix $n = 3, 4$ targets differ only slightly.

Before providing any comments, we note that direct comparisons with observations are not trivial, because of the complexities in line identifications and line blending. Another complexity is due to the temperature sensitivity of the $2s^2\ 2p^4\ 3s \rightarrow 2s^2\ 2p^5$ transitions (pointed out by Cornille et al. 1992), and the fact that the emitting plasma might not be isothermal. In all cases, line ratios were calculated at two temperatures, $\log T(\mathrm{K}) = 6.6, 6.8$, to show the sensitivity of the ratios to the temperature. We note that the APEC isothermal values are very similar to those obtained by Desai et al. (with the exception of the 5–1 transition which is blended with O VIII), who use of an emission measure distribution, strongly peaked at $\log T(K) = 6.8$.

We have also examined the effect of cascading into the levels in our R-matrix ion models. Table 4 shows, for each transition, the ratio of the population of the upper term by radiative cascade to the population due to direct excitation. We see that, for transitions from the $2p^4$ 3d levels, radiative cascade plays a small role compared to direct excitation while the reverse is true for transitions from the $2p^4$ 3s levels. Accordingly, any increase between the intensity ratios of the $n = 3, 4$ R-matrix calculations for the $2p^4$ 3d transitions is due primarily to the additional resonant enhancement of the $n = 4$ calculation. It is a different story for the $2p^4$ 3s transitions where radiative cascades play a large role. The additional level structure of the $n = 4$ calculation is apparent in the increase of the cascade-to-excitation ratio between the $n = 3$ and $n = 4$ intensities. Additional resonant enhancement of the $n = 4$ calculation alone accounts for roughly a 10% increase in the intensity

[1] www.chianti.rl.ac.uk

ratios between the two calculations while we see an overall increase of about 40% for these transitions when including cascade effects. Cascading is also the main reason of the differences between the $n = 3$ distorted wave and $n = 5$ APEC models.

The direct effect of resonanant enhancement can be judged by comparing the results from the two $n = 3$ calculations (R-matrix and distorted wave). Increases up to a factor of two are present for the $2p^4$ 3s transitions. A similar situation occurs between the $n = 4$ R-matrix and the APEC results (the $n = 5$ levels do not have a significant contribution via cascade). Finally, we would like to point out that the intensities of the $2p^4$ 3s transitions are not only affected by resonant excitation and cascading, but also from recombination, as shown by Gu (2003). However, estimates based on the data included in CHIANTI version 5 (Landi et al. 2005) indicate that the inclusion of recombination effects does not significantly affect the line ratios (variations $\leq$10%) for the lines listed in Table 4, with the exception of the 4–1 transition which has increase of 23% at $\log T = 6.8$ when including recombination.

4. Summary

Two R-matrix calculations in intermediate coupling were performed for electron-impact excitation of Fe^{17+}. The effective collision strengths of the $n = 4$ calculation have been archived for all 38 781 inelastic transitions, expanding on the work done in IP XXVIII (Berrington et al. 1998). For the stronger transitions, we find differences in the effective collision strengths on the order of 10% between the two ICFT calculations, while the weakest transitions might differ by up to a factor of 5. The addition of the 2s $2p^5 3l$ and $2p^6 3l$ terms in the present $n = 3$ R-matrix calculation are found to have significant effects on the collision strengths to the $2s^2$ $2p^4 3l$ levels when compared the the R-matrix calculation of Mohan et al. (1987). A low density Fe^{17+} plasma is modeled using the updated collision strengths and compared to spectra calculated using the relativistic distorted wave results of Sampson et al. (1991) and a Chandra observation of Capella. The enhanced collision strengths to the $2s^2$ $2p^4$ 3s levels directly produce an increase in the line intensities of the transitions from these levels. The new collision strengths lead to better agreement with observations.

Acknowledgements. This work has been funded by PPARC grant PPA/G/S2003/00055. GDZ acknowledges support from PPARC.

References

ADAS web page: `http://adas.phys.strath.ac.uk`
Badnell, N. R. 1986, J. Phys. B: At. Mol. Phys., 19, 3827
Badnell, N. R., & Griffin, D. C. 2001, J. Phys. B: At. Mol. Opt. Phys., 34, 681
Berrington, K. A., Saraph, H. E., & Tully, J. A. 1998, A&AS, 129, 161 (IP XXVIII)
Burgess, A. 1974, J. Phys. B: At. Mol. Phys., 7, L364
Burgess, A., Chidichimo, M. C., & Tully, J. A. 1997, J. Phys. B: At. Mol. Opt. Phys., 30, 33
Chidichimo, M. C., Badnell, N. R., & Tully, J. A. 2003, A&A, 401, 1177
Cornille, M., Dubau, J., Loulergue, M., Bely-Dubau, F., & Faucher, P. 1992, A&A, 259, 669
Cowan, R. D. 1981, The Theory of Atomic Structure and Spectra, (California: University of California Press), 569
Desai, P., Brickhouse, N. S., Drake, J. J., et al. 2005, ApJ, 625, L59
Fawcett, B. C. 1984, At. Data Nuc. Data Tables, 31, 495
Griffin, D. C., Badnell, N. R., & Pindzola, M. S. 1998, J. Phys. B: At. Mol. Opt. Phys., 31, 3713
Gu, M. F. 2003, ApJ, 582, 1241
Hummer, D. G., Berrington, K. A., Eissner, W., et al. 1993, A&A, 279, 298
Landi, E., Del Zanna, G., Young, P. R., et al. 2005, ApJ, submitted
Mann, J. B. 1983, At. Data Nuc. Data Tables, 29, 407
Mohan, M., Baluja, K. L., Hibbert, A., & Berrington, K. A. 1987, J. Phys. B: At. Mol. Phys., 20, 6319
NIST web page: `http://physics.nist.gov`
Sampson, D. H., Zhang, H. L., & Fontes, C. J. 1991, At. Data Nuc. Data Tables, 48, 25
Whiteford, A. D., Badnell, N. R., Ballance, C. P., et al. 2001, J. Phys. B: At. Mol. Opt. Phys., 34, 3179